NANO · MICRO small
www.small-journal.com

Introducing Bacteria and Synthetic Biomolecules along Engineered DNA Fibers

Jonathan R. Burns

Deoxyribonucleic acid (DNA) nanotechnology enables user-defined structures to be built with unrivalled control. The approach is currently restricted across the nanoscale, yet the ability to generate macroscopic DNA structures has enormous potential with applications spanning material, physical, and biological science. To address this need, I employed DNA nanotechnology and developed a new macromolecular nanoarchitectonic assembly method to produce DNA fibers with customizable properties. The process involves coalescing DNA nanotubes under high salt conditions to yield filament superstructures. Using this strategy, fibers over 100 microns long, with stiffnesses 10 times greater than cytoskeletal actin filaments can be fabricated. The DNA framework enables fibers to be functionalized with advanced synthetic molecules, including, aptamers, origami, nanoparticles, and vesicles. In addition, the fibers can act as bacterial extracellular scaffolds and adhere *Escherichia coli* cells in a controllable fashion. These results showcase the opportunities offered from DNA nanotechnology across the macroscopic scale. The new biophysical approach should find widespread use, from the generation of hybrid-fabric materials, smart analytical devices in biomedicine, and platforms to study cell-cell interactions.

1. Introduction

Deoxyribonucleic acid (DNA) nanotechnology has produced significant advancements across materials science.[1] The DNA origami construction approach enables discrete structures with nanometer control to be developed readily.[2] The applications are widespread and include robots with programmable movement,[3] DNA-based nanopores with charge selective ion transport,[4] and smart sensing devices which deliver cargo to designated sites in vivo.[5,6] More recently, the field has been expanded towards supramolecular structures which assemble across the low micron scale.[7] Using recognition sites, DNA origami blocks are able to combine into spherical superstructures,[8] organized frameworks can shape lipid vesicles,[9] and plate arrays which assemble on 2D surfaces to mimic famous artwork.[10] This emerging field is opening the way towards novel nanoarchitectonic structures[11] with unique nanoscale functionality. However, expanding this concept further across the micron scale will enable new macromolecular materials to be assembled with unique biophysical control. These materials may include engineered woven fabrics with tailored nano-properties, synthetic actin filaments that simulate cellular movement inside model cells, and extracellular scaffolds which organize cells to aid biomedical research.[12]

DNA-based nanotubes are well suited as nanoarchitectonic structures. DNA strands can be programmed to form extended nanotube lattices. To date, a diverse array of nanotubes have been engineered with controllable diameters and inter-duplex connectivity.[13–17] The arrays can be functionalized and support the 1D organization of metal ions,[18] plasmonic particles,[19] quantum dots,[20] and fluorescent dyes with tailored properties.[21] In addition, DNA nanotubes can be assembled into higher order nanofibers using specially designed junctions or organic modifications.[17,22] However, DNA nanotubes and nanofibers are highly flexible across the micron scale which limits their macroscopic potential. Therefore an alternative strategy is required to rigidify DNA nanotubes.

DNA condensation is a natural phenomenon in cell biology. In order for genomic DNA to fit inside the nucleus of a cell, histone complexes attach to DNA to form a condensed superstructure.[23] This process has been exploited in materials science, for example, Bar-Ziv and co-workers generated 1D patterned bio-chips using spermidine-DNA duplex condensates.[24] Inspired by the favorable properties of condensation, I have developed a novel macromolecular assembly method which condenses flexible DNA nanotubes into rigid fibers (**Figure 1**). Applying high concentrations of divalent metal cations generates an inter-nanotube complex (Figure 1a, inset). The component nanotube was first presented by Winfree and co-workers[13] and is assembled from subunits comprised of five oligonucleotides. Complementary toe-hold single strands positioned at each corner of the subunit overlap with a pitch of ≈30° to form, on average, a 7 subunit, 14 helix bundle. The bundles elongate upon annealing to generate a flexible nanotube framework (Figures S1–S3, Supporting Information).

Dr. J. R. Burns
Department of Chemistry
Institute of Structural and Molecular Biology
University College London
London WC1H 0AJ, UK
E-mail: jonathan.burns@ucl.ac.uk

The ORCID identification number(s) for the author(s) of this article can be found under https://doi.org/10.1002/smll.202100136.

DOI: 10.1002/smll.202100136

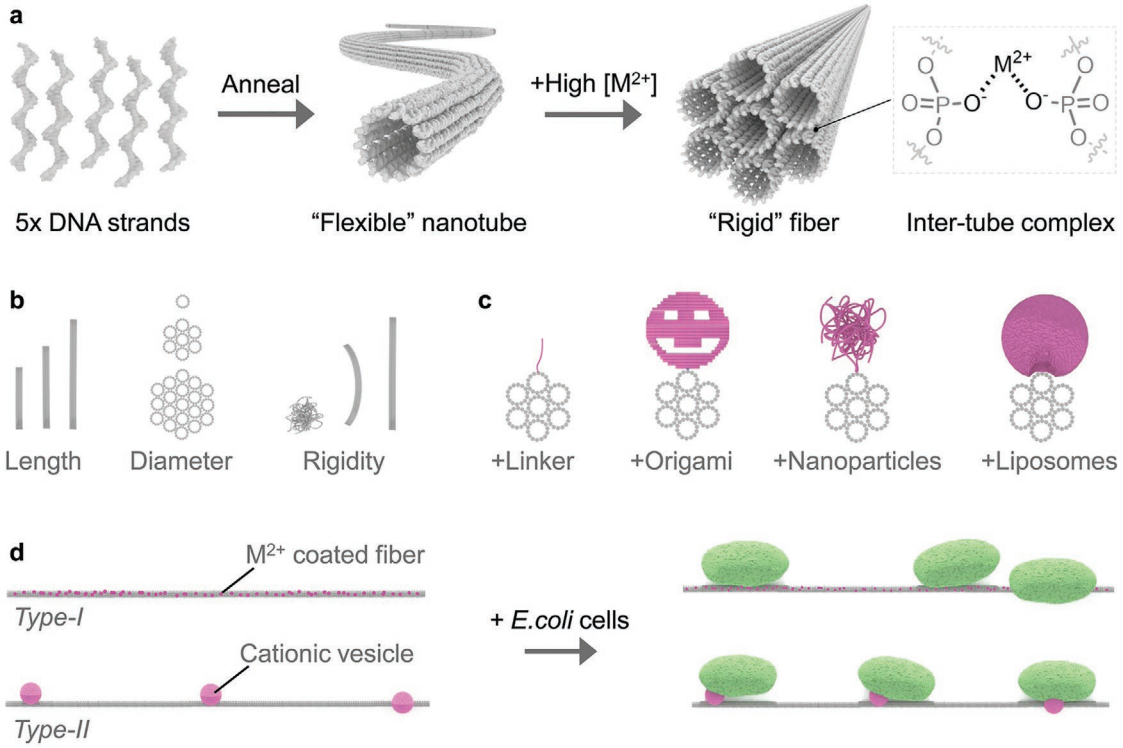

Figure 1. Overview of engineered DNA fibers. a) Five component oligonucleotides anneal to form flexible DNA nanotubes under low salt conditions, or highly rigid DNA fibers (grey) in the presence of high concentrations of divalent metal cations, chemical structure of fiber inter-nanotube metal complex (inset). b) Fibers are highly versatile and can be customized in length, diameter, and rigidity. c) Fibers can be decorated with advanced synthetic molecules, including, DNA linkers, DNA origami, DNA nanoparticles, and liposomes (magenta). d) *E. coli* cells (green) adhere to DNA fibers using two approaches, via divalent metal cations (type-I, magenta dots) or cationic vesicles (magenta spheres) (type-II).

Structural analysis of the nanotubes and fibers was conducted first to identify their core parameters, including, diameter, length, and rigidity (Figure 1b). The superstructures' metal cation concentration dependency was established, along with annealing profiles, optimal annealing rates, and biocompatibility. Next, their modular properties were studied, and how the introduction of π-stacking cyanine dyes, or multiple seed-annealing cycles influences fiber formation. Following this, the fiber assembly process was applied to different DNA nanotube designs to confirm the methodology is generalizable. To showcase the DNA-enabled approach, a range of advanced synthetic biomolecules were incorporated (Figure 1c). The engineered filaments were then used to bind bacteria cells to function as extracellular scaffolds (Figure 1d). Two cell adhering mechanisms were investigated, either using divalent metals cations (type-I) or cationic liposomes (type-II). Finally, advanced bacterial cell matrix applications were developed, including adhesion under complex multicellular conditions to organized cell division along the framework.

2. Results

2.1. Structural Characterization of DNA Nanotubes and Fibers

The DNA framework must be sufficiently stable and rigid across the micron range for macroscopic applications. To achieve this, individual DNA nanotubes were coalesced into structurally more rigid and longer fibers. Experimental characterization showed isolated DNA nanotubes form readily after mixing the 5 component strands and annealing less than 1 h in buffer containing 14 mM $MgCl_2$ (see Figures S1–S3,S7–S12, Tables S1–S3, Supporting Information). Transmission electron microscopy (TEM) and confocal laser scanning microscopy (CLSM) confirmed the DNA nanotube formation (**Figure 2**a; Figures S12–S15, Supporting Information). Nanotubes with diameters between 7 and 20 nm are observed, which is comparable to previously published results.[13] However, the frameworks are highly flexible and formed large interwoven bundles measuring ≈6 µm across (Figures S12–S15, Supporting Information). The nanotubes physical properties are shown in **Table 1**.

At high divalent metal ion concentrations the DNA nanotubes coalesced to form highly rigid fibers (Figure 2b; Figures S9–S11, Supporting Information). Structural characterization revealed long filaments were generated when the component mixture was annealed in at least 42 mM $MgCl_2$ or $CaCl_2$ (Figure S9, Supporting Information). TEM analysis showed fibers are composed of tightly packed and aligned DNA nanotubes (Figure 2b-ii; Figures S12,S13, Supporting Information). The filaments measure ≈7 nanotubes across, implying each fiber is a bundle of ≈37 condensed nanotubes. The nanotube packing arrangement was due to high concentrations of divalent metal cations which complex between adjacent phosphate anions from neighboring nanotubes (Figure 1a, inset). The divalent requirement was confirmed since monovalent NaCl and KCl

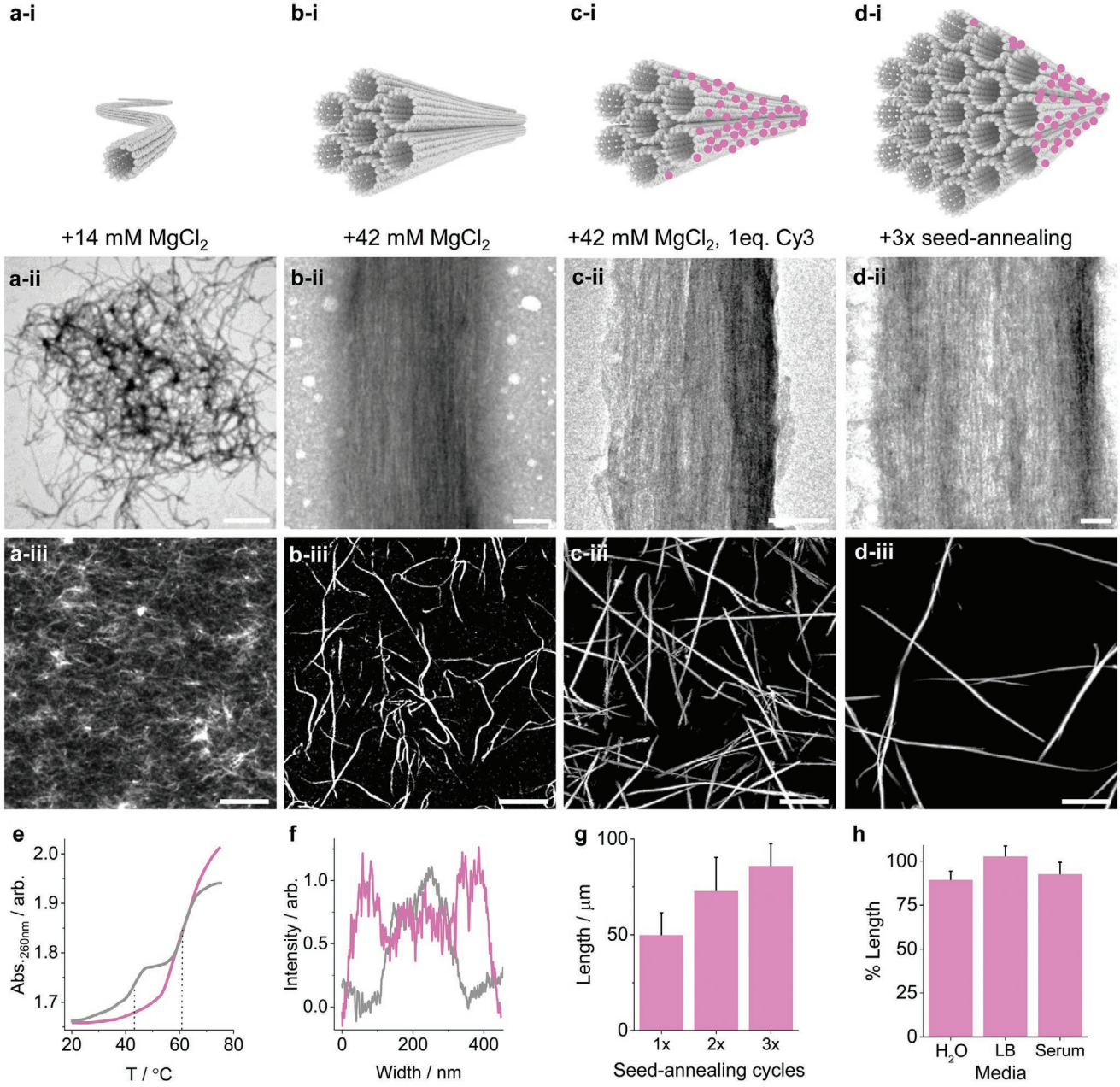

Figure 2. Structural characterization of DNA nanotubes and fibers. a) DNA nanotubes; a-i) 3D rendering, a-ii) TEM image of nanotube bundle, scale bar 1000 nm, and a-iii) CLSM showing ensemble nanotube bundles, scale bar 10 µm. b) DNA fibers; b-i) 3D rendering, b-ii) TEM image of fiber, scale bar 50 nm, and b-iii) CLSM image showing ensemble fibers, scale bar 10 µm. c) Ultra-rigid DNA fiber characterization using 1 eq. of Cy3 modification per subunit (magenta spheres); c-i) 3D rendering, c-ii) TEM image of fiber cross-section, scale bar 50 nm, and c-iii) CLSM image showing ensemble fibers, scale bar 10 µm. d) Ultra-long DNA fiber characterization with multiple seed-annealing cycles containing 1 eq. of Cy3 modifications per subunit (magenta spheres); d-i) 3D rendering, d-ii) TEM image, scale bar 50 nm, and d-iii) CLSM image of ensemble fibers, scale bar 10 µm. e) UV absorbance thermal analysis at 260 nm comparing annealing (grey line) and melting transitions (magenta line) of DNA fibers, dotted lines represent the T_m values. f) TEM cross-section width analysis comparing DNA fibers without (grey line) and with 3× seed-annealing cycles (magenta line). g) CLSM-derived length analysis of DNA fibers with various seed-annealing cycles, values obtained by plotting the average longest fibers for each cycle. h) CLSM-derived stability of DNA fibers in deionized water (H_2O), lysogeny broth (LB), and fetal bovine serum (Serum), values represent the percentage length after 4 h exposure at 37 °C.

did not form fibers (Figure S9, Supporting Information). CLSM showed the fibers measure up to 33.3 µm ± 3.7 µm (Figure 2b-iii), and are almost an order of magnitude stiffer than isolated nanotubes (Table 1; Figures S14,S15, Supporting Information). Agarose gel electrophoresis and a centrifugal pelleting assay confirmed the fibers form in high ratios (Figures S7,S8, Supporting Information). Gel electrophoretic analysis showed the fibers did not migrate into the gel lane. This indicates the majority of the component oligonucleotides and subunits formed a large molecular weight complex. A centrifugal

Table 1. Physical properties of DNA nanotubes and fibers.

Construct	Maximum length [μm]	Persistence length [μm]	T_m ([°C]
DNA nanotubes	-	2.0 ± 0.1	47.1, 62.0
DNA fiber 0.1 eq. Cy3	33.3 ± 3.7	17.9 ± 1.7	61.1
DNA fiber 1 eq. Cy3	40.6 ± 6.3	217.2 ± 31.4	63.0
3× seed-anneal DNA fiber 1 eq. Cy3	101.1 ± 29.8	272.8 ± 13.8	–

pelleting assay backed up this finding which revealed 90.3 ± 2.3% was large enough to precipitate under modest centrifugal forces.

The condensation strategy is compatible with other DNA nanotube designs. A tile[16] and origami-based[25] nanotube designs were assayed and their fiber-forming properties identified (Figure S16, Supporting Information). The DNA tile is assembled from overlapping subunits, whilst the DNA origami structure contains terminal blunt-ends which interact with other subunits to form a nanotube array. CLSM showed both types of nanotubes were able to form fibers under high divalent metal ion concentrations, to confirm the condensation approach is generalizable.

The fibers' length and stiffness can be improved by introducing high concentrations of aromatic fluorophores (Figure 2c). Cy3 is known to form homodimers via favorable π-stacking interactions.[26] Increasing the modified DNA concentration from 0.1 to 1 μM, which equates to 0.1 and 1 Cy3 per subunit, respectively, increased the length and rigidity of fibers markedly. TEM analysis showed the fibers formed tightly bound nanotube complexes with co-aligned subunits (Figure 2c-ii; Figures S12,S13, Supporting Information). CLSM identified the longest fibers' increased to over 40 μm, whilst the persistence length increased to over 200 μm (Figure 2b-iii, Table 1; Figure S14, Supporting Information), which is an order of magnitude stiffer than cytoskeletal actin filaments.[27] The results imply the Cy3 dyes interact constructively in the nanotube bundle with adjacent dyes via π-stacking interactions. A similar stabilizing effect has also been observed for other covalently attached aromatic modifications on DNA, including porphyrins.[28]

Thermal UV absorbance and corresponding CLSM analysis confirmed all DNA constructs remain structurally stable at physiological temperatures (Figure 2e, Table 1; Figure S17, Supporting Information). The DNA nanotubes and fibers were folded by thermally annealing between 75 and 20 °C at a rate of 1 °C min^{-1}. Monitoring the absorbance at 260 nm, the annealing profiles revealed a 2-step transition for all constructs. Previously published results[13,29] show the core subunit has a melting temperature between 50 and 55 °C, which corresponds to the higher melting transition. Whilst the four toe-hold single strands around each subunit, which are five bases long, give rise to the lower melting transition. Upon cooling, the subunit toe-holds anneal with other subunits to form a 1D nanotube lattice. The mechanism of nanotube-lattice formation has been shown to follow a nucleation-elongation model.[16] This result implies both the nanotubes and fibers form simultaneously, and therefore also follows a nucleation-elongation mechanism (Figures S17,S18, Supporting Information). Contrastingly, in the melting profiles, only DNA nanotubes displayed a 2-step melting transition (T_m) (47.1 and 62.0 °C), whilst the fibers displayed a single melting transition (61.1–63.0 °C). The high thermal stability of the fibers indicates they form highly cooperative superstructures suitable for various bionanotechnology applications.

The fibers' length and diameter can be improved by performing multiple seed-annealing cycles (Figure 2d; Figure S19, Supporting Information). The large hysteresis shift between the annealing temperature (≈47 °C) and the melting temperature (≈62 °C) can be exploited, enabling assembled fibers to be combined with additional component strands at 55 °C. Upon cooling, the supplemented oligonucleotides complex to the annealed fibers to increase their length and width markedly (Figure 2g). Using this strategy, the fibers' dimensions can be modulated by varying the number of seed-annealing cycles. 3× seed-annealing cycles improved the fibers' stiffness further, with fibers over 100 μm long and 300 nm wide observed (Table 1; Figures S12–S14, Supporting Information).

DNA fibers are stable in biocompatible cell media and displayed good nuclease resistance properties. The fibers were pelleted and resuspended in lysogeny broth (LB) or fetal bovine serum, and the length monitored using CLSM (Figure 2h; Figures S20,S21, Supporting Information). After 4 h, the length was measured to be >80% of the original. This result confirmed the fibers remain stable and resilient to physiological temperatures and proteins in both media types, including DNA digestion enzymes within this timeframe. The fibers also remain stable when resuspended into deionized water.

2.2. Functionalizing DNA Fibers with Synthetic Biomolecules

DNA fibers can be modified with a range of biomolecules to introduce nanoscale functionality. Firstly, DNA single-strand linkers were incorporated to enable subsequent downstream DNA attachment (**Figure 3**a; see Tables S1–S3, Supporting Information for sequences and mixing, and Figure S4, Supporting Information for 2D strand map). The extended linker strand contains the DNA sequence of a component oligonucleotide, but extended in the 5′ direction, leaving a single strand domain protruding from the fiber. TEM and CLSM showed the linker strands did not interfere with fiber formation, even when added in a one equivalent stoichiometric ratio per subunit (Figure 3a-ii–iv; Figures S22,S23, Supporting Information). The linker regions can be used as aptamer sequences to direct cellular binding,[30] or as DNAzymes to introduce subsequent mechanical action.[31]

Secondly, DNA origami nanostructures can be attached to fibers via single strand linkers (Figure 3b). A dye-labeled DNA origami smiley measuring ≈90 nm × 70 nm × 2 nm was incorporated into the DNA fibers by mixing the two folded and purified constructs (see Figure S5, Supporting Information for 2D strand map, and Table S4, Supporting Information for sequences, Figure S24, Supporting Information). Atomic force microscopy (AFM) and CLSM confirmed the two synthetic biomolecules were able to assemble readily, and that the DNA origami was able to tether specifically to the fibers (Figure 3b-ii–iv; Figure S25, Supporting Information). A control fiber without

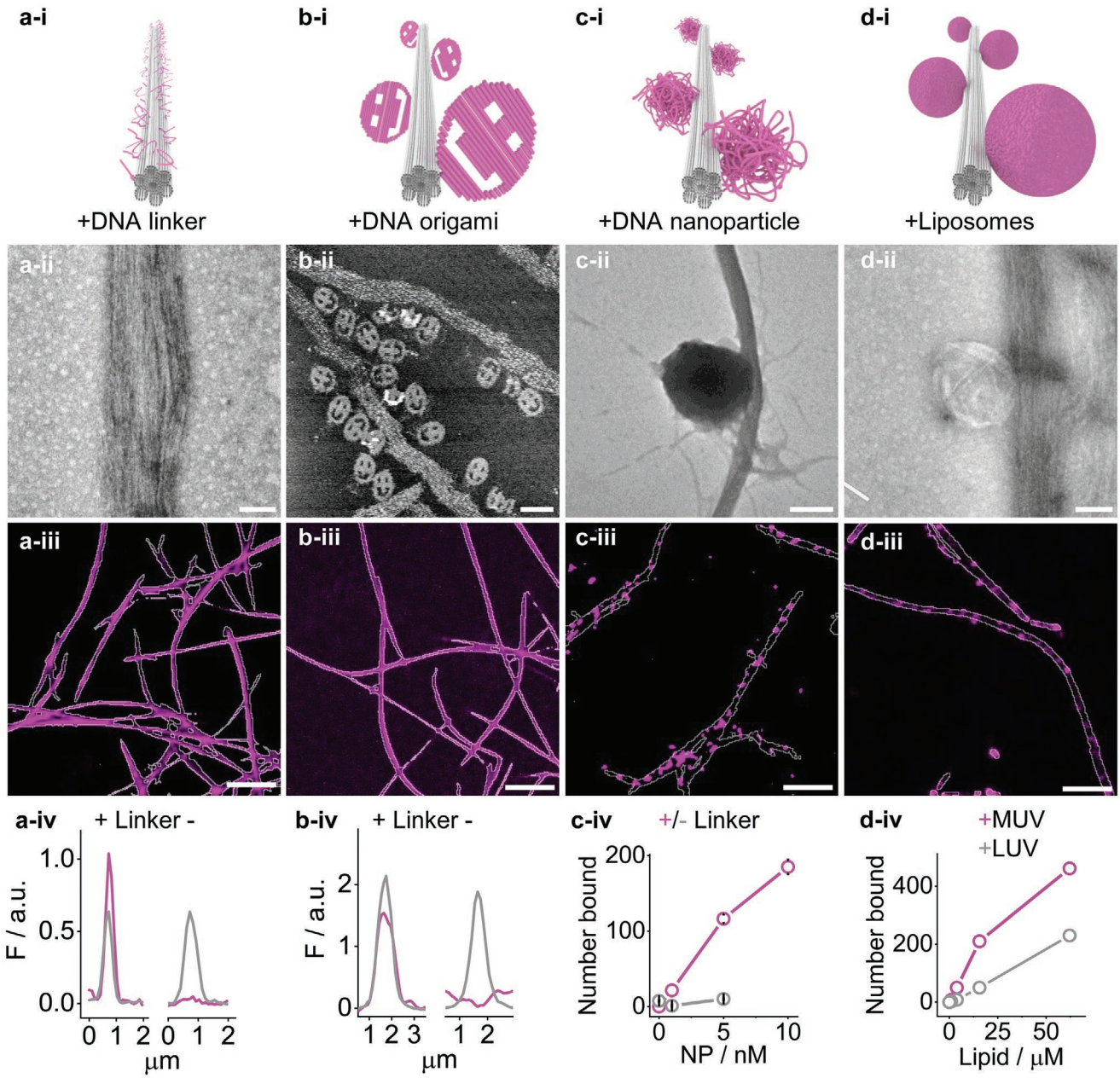

Figure 3. Functionalizing DNA fibers with synthetic biomolecules. a) Characterization of DNA fibers (grey) modified with linker strands (magenta) extended from component oligonucleotides, corresponding a-i) 3D rendering, a-ii) TEM image, scale bar 100 nm, a-iii) CLSM image of DNA fibers (grey channel) with fluorescein labeled-linker strands (magenta channel), scale bar 10 µm, and a-iv) cross-sectional analysis of CLSM images comparing DNA fibers (grey line) with and without linker strands (magenta line). b) Characterization of DNA fibers (grey) modified with fluorescein-labeled DNA origami smileys (magenta) connected via linker strands, corresponding b-i) 3D rendering, b-ii) AFM image of ruptured nanotubes, scale bar 100 nm, b-iii) CLSM image of DNA fibers (grey channel) with linker strands and DNA origami smileys (magenta channel), scale bar 10 µm, and b-iv) cross-sectional analysis of CLSM images comparing DNA fibers (grey line) with and without linker strands containing DNA origami smileys (magenta line). c) Characterization of DNA fibers (grey) modified with Cy5-labelled hydrophobic DNA nanoparticles (magenta) connected via linker strands, corresponding c-i) 3D rendering, c-ii) TEM image, scale bar 100 nm, c-iii) CLSM image of DNA fibers (grey channel) with linker strands and DNA nanoparticles (magenta channel), scale bar 10 µm, and c-iv) CLSM analysis comparing number of DNA nanoparticles bound along DNA fibers with (magenta line) and without linker strands (grey line). d) Characterization of DNA fibers (grey) complexed with vesicles (magenta) of different sizes, corresponding d-i) 3D rendering, d-ii) TEM image, scale bar 100 nm, d-iii) CLSM image of DNA fibers (grey channel) complexed with MUVs (magenta channel), scale bar 10 µm, and d-iv) CLSM analysis comparing the number of bound SUVs (grey line) versus MUVs (magenta line) along DNA fibers (grey line) with increasing concentration.

the linker strands did not show any significant DNA origami loading, confirming the two complementary strands extended from the fiber and origami were able to form a stable duplex. This result means the DNA matrix can be decorated with a vast array of complex structures, from sensors,[5] robots,[3] or quantum dot-loaded motifs.[20]

Thirdly, hydrophobic DNA nanoparticles were able to bind along the DNA framework via single strand linkers (Figure 3c). DNA nanoparticles containing cholesterol-rich regions were generated from M13mp18 single strands (see Figure S6, Supporting Information for 2D strand map and Figure S26, Supporting Information, Tables S1–S3,S5, Supporting Information for sequences and mixing). Cholesterol-modified oligonucleotides were introduced to the scaffold by binding to 34 target sites using 17 helper strands. The embedded cholesterols interact with other functionalized scaffolds via favorable hydrophobic intermolecular interactions to form nanometer-sized particles. A single strand region of the M13mp18 scaffold was designed to tether to the extended linking strand from the fiber. TEM and CLSM showed the DNA nanoparticles were able to bind along the fiber via the linker strand (Figure 3c-ii–iv; Figures S27,S28, Supporting Information). The role of the linker strand was confirmed since a control fiber without the linkers showed significantly less nanoparticle loading. The DNA nanoparticles may serve as sensitive functional sensors to support biomedical research along fibers.[32]

Finally, DNA fibers can be decorated with liposomes of various diameters (Figure 3d). Liposomes composed of lipid 1,2-dimyristoyl-sn-glycero-3-phosphocholine (DMPC) complexed to DNA fibers via favorable ionic interactions. Vesicles ranging from 100 nm to 20 μm in diameter were screened and the fiber-loading capabilities determined. TEM and CLSM showed the liposomes complex readily to the fibers (Figure 3d; Figures S29,S30, Supporting Information). Small, medium, and large unilamellar vesicles (S-, M-, and LUVs), with diameters of 100, 400, and 1000 nm, respectively, align along the 1D arrays. In contrast, giant unilamellar vesicles (GUVs), with diameters between 2 and 20 μm, were too large to align, and instead caused the fibers to wrap around the vesicles. The binding event was mediated via magnesium ions since a control assay using potassium ions did not show any vesicle loading. This result confirmed magnesium ions coordinate between negatively charged phosphate anions from the DNA and DMPC lipid headgroups. The immobilized liposomes can be used to direct binding via lipid modified headgroups, or as active ingredient reservoirs for downstream cell-matrix applications.[33]

2.3. *Escherichia coli* Cells Adhere Along DNA Fibers

In order to study bacterial cell adhesion, DNA fibers were first bound to a glass microfluidic chamber. The fibers aligned under flow by applying shear stress forces. Time-series CLSM analysis showed fibers adhered rapidly to the glass surface and orientated with the flow direction (see Figure S31, Supporting Information). The aligned fibers average length was 57.2 (± 30.2) μm long.

Divalent metal cations mediate *Escherichia coli* cell binding along flow-aligned fibers following a type I mechanism (Figure 1d). In nature, neutrophils excrete DNA to act as extracellular traps to capture Gram-negative pathogens in the presence of divalent metal ions[34] Inspired by this process, magnesium and calcium ions were employed to mediate binding between negatively charged phosphates from the fiber, and negatively charged entities from the outer membrane of *E. coli*, including phosphatidylglycerol (PG) lipids and glycocalyx groups (**Figure 4**a).[35] TEM analysis showed the fibers were able to complex *E. coli* cells along the 1D array in the presence of these cations (Figure 4b; Figure S32, Supporting Information). The images also revealed the fibers remained structurally rigid during the complexation process and can support micron-sized bacteria cells. Next, CLSM was used to investigate the cation binding dependency of *E. coli* cells. Three salt conditions were screened to identify the optimal cell loading (Figure 4c,d; Figure S33, Supporting Information), divalent magnesium and calcium ions, and monovalent potassium ions. Calcium ions only caused the *E. coli* cells to clump together and were therefore not suitable for comparison. Using flow-aligned fibers, combined calcium and magnesium ions exhibited the most efficient *E. coli* cell complexation properties. The cell loading was 6.4 times higher than magnesium ions. Whilst potassium ions did not show any significant binding to confirm the divalent requirement. CLSM also revealed the cell binding event is rapid. Analysis of the combined entities in the presence of magnesium and calcium ions showed complexation occurred within seconds using a microfluidic flow chamber. Once bound, particle tracking analysis showed the cell remained fixed at the fiber site (Figure S34, Supporting Information).

Cationic liposomes support type II *E. coli* cell adhesion along DNA fibers. Positively charged lipids were introduced into liposomes to mediate binding between negatively charged DNA fibers and *E. coli* cells (Figures 1d,4e).[36] First, the optimal cationic-vesicle fiber loading ratio was identified using CLSM (see Figure S30, Supporting Information). This was performed to ensure the vesicles remain isolated along the fibers. Next, bovine serum albumin (BSA) was added to the reaction mixture to minimize cellular binding via Mg^{2+} ions. BSA also prevented the fibers from sticking to the glass surface, which had the added benefit of improving its molecular accessibility to freely diffusing cells. TEM and CLSM images showed the *E. coli* cells bind only at the vesicle sites along the DNA fiber (Figure 4f,g; Figures S35,S36, Supporting Information). Two different 1,2-dioleoyl-3-trimethylammonium-propane (DOTAP)-containing vesicle sizes were assayed, 100 nm SUVs and 400 nm MUVs. The analysis revealed the smaller vesicles were not suitable for location-specific cellular binding, as each cell was able to bind to more than one vesicle along the fiber. In contrast, the larger vesicle size showed improved binding properties, where each cell was able to adhere to one vesicle along the fiber. Time-series particle tracking analysis showed the bound cells remained tethered but was able to diffuse around the liposome (Figure 4h; Figure S37, Supporting Information). The rotational movement was most likely due to lipid diffusion from the vesicle and cell membranes.[37] Using this approach, the intercellular spacing between the immobilized cells was identified. Gap analysis revealed the cells fluctuated with low micron-scale mobility.

2.4. Biological Applications of *E. coli*-DNA Fibers

DNA fibers can function as advanced extracellular scaffolds. The fibers can act as bacteria-capture devices and were able to bind *E. coli* cells under complex biological conditions. To test

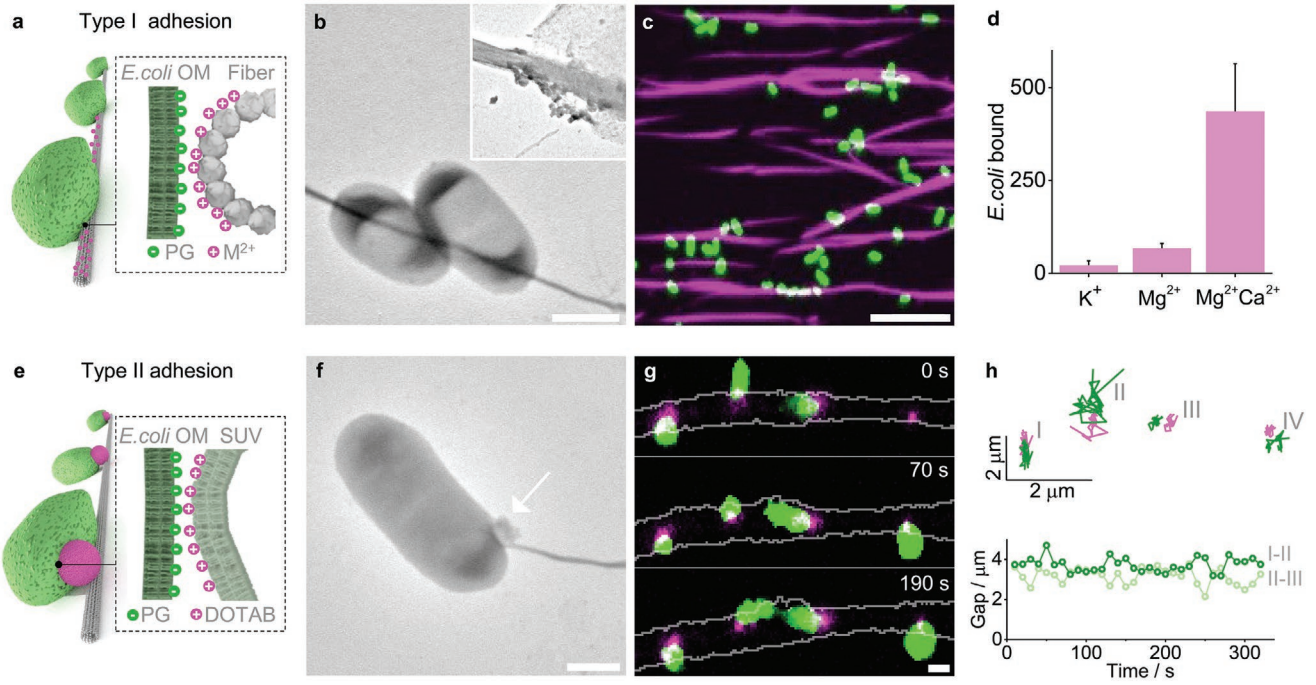

Figure 4. *E. coli* cells adhere along DNA fibers. Type I cell adhesion mediated via Mg^{2+} and Ca^{2+} ions between DNA fibers (grey) and phosphatidylglycerol (PG) lipids found in the outer membrane (OM) of *E. coli* cells (green), corresponding a) 3D representation of complex, b) TEM image of fiber-*E. coli* complex in Mg^{2+} and Ca^{2+} solution, scale bar 1 µm, insert magnification of complex, c) CLSM image of flow-aligned fibers (magenta channel) complexed with *E. coli* cells (green channel) in Mg^{2+} and Ca^{2+} solution, scale bar 10 µm, and d) fiber counterion dependency of bound *E. coli* cells derived from CLSM analysis. Type II cell adhesion mediated via cationic liposomes (magenta) between negatively charged DNA fibers (grey) and phosphatidylglycerol (PG) lipids found in the OM of *E. coli* cells (green), corresponding e) 3D rendering of complex, f) TEM image of *E. coli*-SUV-fiber, arrow denotes the position of the vesicle, scale bar 1 µm, g) CLSM time series of *E. coli* cells (green channel) adhering at cationic SUVs (magenta channel) tethered to DNA fibers (grey channel), scale bar 1 µm, and h) particle tracking analysis of tethered *E. coli* cells (green) with SUVs (magenta) (top), and corresponding gap separation between cells (bottom) taken from (g).

the cellular selectively, fibers were added to *E. coli* cells mixed with dilute whole blood (WB) in reduced serum media. Using a microfluidic chamber, CLSM revealed DNA fibers adhered *E. coli* cells and not erythrocytes or white blood cells (**Figure 5**a; Figure S38, Supporting Information). This selectivity was most likely due to blood cells having reduced levels of negatively charged lipid molecules compared to *E. coli*.[35] In addition, the analysis also confirmed the binding was maintained in the presence of serum proteins. At high concentrations the fibers formed 3D networks to act as conventional extracellular

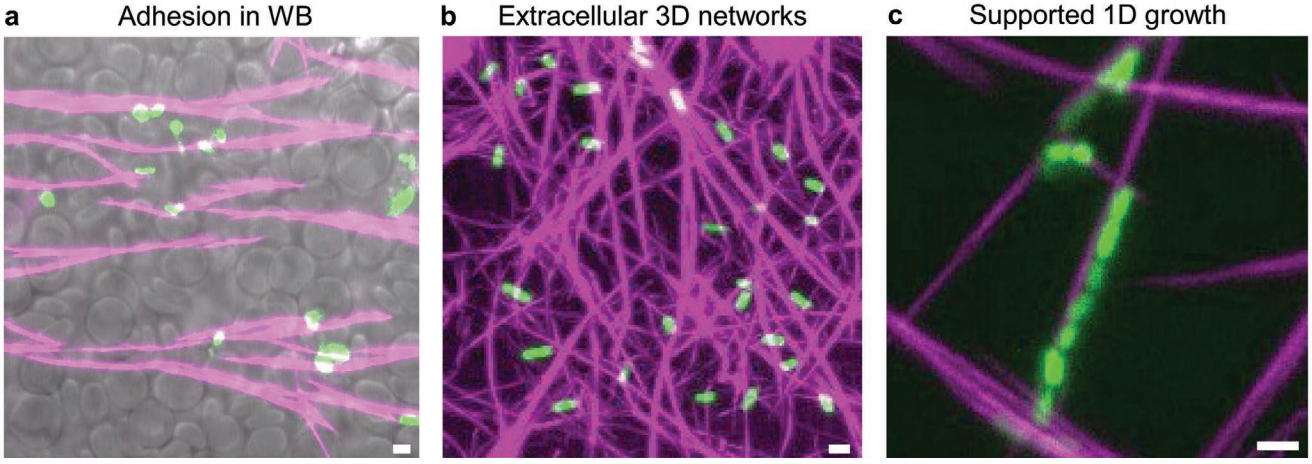

Figure 5. Applications of extracellular DNA fibers. a) DNA fibers (magenta channel) selectively adhere *E. coli* cells (green channel) and not erythrocytes or white blood cells found in whole blood (WB, bright-field channel) in reduced serum via a type I mechanism using Ca^{2+} and Mg^{2+} ions, scale bar 2 µm. b) 3D DNA fiber matrix (magenta channel) adheres *E. coli* cells via a type I mechanism using Ca^{2+} and Mg^{2+} ions, scale bar 2 µm. c) Over time DNA fibers can support multi-generational alignment of dividing *E. coli* cells, scale bar 2 µm.

matrices.[38] This approach can also be used to mimic extracellular DNA which is used by certain bacterial strains during biofilm formation.[39] CLSM showed the fibers form interconnected frameworks when left to settle on a surface at 1 μM or higher. When *E. coli* cells were added to Mg^{2+} and Ca^{2+} coated fibers, the cells adhered readily via a type I mechanism (Figure 5b; Figure S39, Supporting Information). Importantly, the bound cells were viable for both adhesion mechanisms. Times series analysis confirmed the vesicle-fused cells were viable (Figure S40, Supporting Information). After 29 min of cell adhesion, the images showed the *E. coli* cells were able to divide at the vesicle site. Contrastingly, for calcium and magnesium mediated adhesion, the dividing cells remained complexed to the extracellular scaffold in some instances. Using non-flow aligned fibers, CLSM showed the cells were able to divide sequentially along the DNA framework (Figure 5c; Figure S41, Supporting Information). The image revealed the 1D array was able to sculpt the dividing daughter cells to enable long-term multi-generational order.

3. Summary and Perspective

A new macromolecular nanoarchitectonic approach has been developed which can be functionalized with synthetic biomolecules and *E. coli* cells. The findings expand the boundaries of DNA nanotechnology by generating highly functional macroscopic fibers. The results show DNA nanotube condensation is very efficient, robust, and versatile. The strategy is generalizable as both DNA origami and tile-based nanotube designs can be condensed into fibers. Modifying the surface chemistry of the fibers by introducing π-stacking modifications, or adapting the annealing protocol, enables the diameter, length, and rigidity to be customized. However, there is scope to expand the properties further, for instance, applying more seed-annealing cycles should yield even longer and stiffer fibers. Alternative condensation agents, like diverse divalent metal cations or small cationic organic molecules[24] can enhance the fibers chemical diversity. DNA fibers may be simplified by using nanotubes comprised of just one oligonucleotide.[15] Or contrastingly, employing origami-based designs, which exploit secondary structure-recognition,[8] may facilitate sequence-specific control across the entire fiber length.

The biophysical ability to organize bacteria cells along DNA fibers should find widespread use in biomedical research.[40] The results show DNA fibers' capture selectivity is maintained in complex biological systems paving the way for future clinical applications, including, novel wound-dressing materials to dialysis devices.[41] The intercellular-gap analysis between tethered *E. coli* cells reveals their position is relatively fixed along the framework. This ability means the proximity between bound cells can be determined and important studies performed, such as, distance thresholds for cell-cell communication, the generation of complex 3D cell matrixes to mimic biofilm formation,[42] and aligned multi-generational cell experiments to study antimicrobial resistance.[43] Incorporating advanced synthetic biomolecules along the DNA framework can help support mechanistic research, or be used to direct cell-specific binding. Smart molecules readily incorporated include, DNA aptamers, DNA origami-based robots, or liposome agents, all of which can be activated to release payloads on command. In addition, the extracellular scaffold can be selectively digested by applying a high concentration of DNase enzymes. These advanced matrix properties are not readily possible with existing extracellular scaffolds.

In synthetic biology, new functional materials can be developed, including replicating actin filaments inside model cells with controlled cellular movement, to mimicking flagella motion of synthetic bacteria. Alternatively, with bigger and stiffer fibers, the arrays should be able to support mammalian cells, opening the route for unique cell-, skin-, and organ-grafting materials.[44] Additionally, the DNA fibers have a densely packed core, which could be used as novel drug delivery agents, similar to DNA hydrogels.[45] Importantly, the unit cost of the DNA framework is relatively cheap, requiring just 5 component single strands, meaning the new materials can be applied to many approaches at scale. To complement this, the fibers can be pelleted readily using centrifugation, and therefore concentrated, diluted, or exchanged into new buffer systems in seconds. In conclusion, my report advances the field of macromolecular nanoarchitectonics across three disciplines, and helps to address the demand for macroscopic materials with nanotechnology-enabled functionality.

4. Experimental Section

Reagents: All DNA oligonucleotides were purchased from IDT DNA technologies (Coralville, IA, USA) on a 250 nmol scale, desalted, except cholesterol and Cy3 modified DNA which was purified with HPLC. All other reagents were purchased from Sigma Merck (UK) unless stated.

Folding Nanotubes and Fibers: The DNA nanotube was published previously (information on the sequences, and mixing, including 2D maps and dimensions is provided in Tables S1–S3, Supporting Information).[13] The tubes and fibers were assembled by combining an equimolar mixture of the component DNA strands (at 1 or 10 μM, 1000 μL, unless stated) in 1× TAE pH 8.3 with 14 mM $MgCl_2$ for nanotube formation, or 42 mM $MgCl_2$ for fiber formation (unless stated). The constructs were folded by heating the solution at 95 °C for 2 min, then cooling to 60 °C at a rate of 5 °C min^{-1}, and then to 20 °C at a rate of 1 °C min^{-1}. Folding was performed in plastic PCR tubes (100 μL) using a PCR instrument (BioRad, UK). For AFM analysis of DNA nanotubes, the constructs (1 μM, 100 μL) were ligated to prevent rupturing by adding T4 kinase buffer (10×, 10 μL, New England Biolabs, UK), T4 kinase (10 000 U mL^{-1}, 1 μL, New England Biolabs, UK) and T4 ligase (2 000 000 U mL^{-1}, 1 μL, New England Biolabs, UK) overnight.

Purification of Fibers: The fibers (1 or 10 μM, 1000 μL) were washed by combining the samples in a plastic vial (1 mL, Eppendorf, UK), and centrifuging for 4 min at 16k r.p.m. The supernatant (900 μL) was removed and replaced with fresh folding buffer (900 μL). The washing step was repeated two more times, and the fiber resuspended with mixing. The pure constructs were stored at room temperature, used within two weeks and mixed prior to use by shaking for 2 s.

Transmission Electron Microscopy: Carbon-coated copper grids (EM resolutions, UK) were glow discharged for 90 s (Quorum, UK). The DNA nanotubes or fibers (10 μL, 1 μM, in folding buffer) were deposited on the grid for 1 min. The grid was then added to a uranyl formate droplet (10 μL, 2% w/v in deionized water) for 1 s, transferred to a second uranyl formate droplet (10 μL) for 1 s, and then washed by placing in a deionized water droplet (10 μL) for 1 s. Finally, the grid was dried by blotting onto filter paper and applying a gentle airflow for 1 min. The samples were imaged using a transmission electron microscope (JEM-2100, Jeol, US) equipped with a camera (SC200, Gatan Orius, US).

Confocal Laser Scanning Microscopy: CLSM images were collected using a 60× oil objective microscope (FV-1000 Olympus, UK). To visualize the folded nanotubes and fibers, the DNA solution (10 µL, unless stated at 1 µM in folding buffer) was deposited on a fluorodish (World Precision Instruments, Sarasota, FL, USA) and left to settle for 5 min before imaging. Where possible, the microscope settings were kept identical for each experiment. Images were maximum projections from a z-stack, except for times series videos which are single frames collected with a wide aperture. The images were analyzed using ImageJ software (https://imagej.nih.gov/ij/). The contour lengths and longest fibers were measured using the line segmentation tool in ImageJ and then averaged. The persistence lengths were calculated using the Persistence Version 4 software.[46]

Agarose Gel Nanotube and Fiber Analysis: The nanotubes and fibers (10 µL, 1 µM, in TAE pH 8.3, folded in 14, and 42 mM $MgCl_2$, respectively) were added to purple gel loading dye (10 µL) (New England Biolabs, UK), and loaded onto a 4% agarose gel containing 1× TAE with 2 mM $MgCl_2$ and ethidium bromide. The gel was run at 60 volts for 1 h at 4 °C and visualized using a gel reader.

UV Melting Studies: Thermal melting studies were performed using a UV–vis spectrophotometer (Varian Cary Eclipse, Agilent, UK) by monitoring the absorption at 260 nm of DNA nanotubes (1 µM, 1 mL, 1× TAE pH 8.3, and 14 mM $MgCl_2$) and DNA fibers (1 µM, 1 mL, 1× TAE pH 8.3, 42 mM $MgCl_2$) in a 1 cm quartz cuvette. Heating and annealing was performed in 1 °C steps for 1 min between 75 and 20 °C.

Ultra-Long and Wide DNA Fibers: The DNA fibers were folded following the protocol described above (1 µM, 1000 µL), then concentrated by centrifuging for 4 min at 16k r.p.m. to generate a pellet. The supernatant (800 µL) removed and the fiber was resuspended by shaking the remaining solution (≈5 µM, 200 µL). Next, the assembled fiber solution (5 µM, 25 µL) was used as a seed and added to annealing fiber (5 µM, 25 µL) at 55 °C. Upon cooling, longer and wider fibers were generated. The seeding process was repeated a two more times to generate even longer and wider fibers.

DNA fiber Buffer Exchange and Stability Assays: To freshly assembled and washed DNA fibers (100 µL, folded at 1 µM, in 1× TAE pH 8.3, and 42 mM $MgCl_2$) the solution was centrifuged for 4 min at 16k r.p.m., and the supernatant carefully removed (90 µL). The stated buffer system (90 µL) was then added to the pelleted fiber and the solution mixed to re-suspend the DNA fiber. CLSM images were collected 4 h after buffer transfer.

DNA Origami Preparation: M13mp18 single strand scaffold (125 µL, 50 nM) was added to the staple strands (200 µL, 250 nM, see Table S4, Supporting Information for sequences), 10× TAE pH 8.3 (100 µL), $MgCl_2$ (1000 mM, 14 µL), and water (561 µL). The origami was folded by thermally annealing the mixture from 70 to 30 °C for 2 h. Excess staple strands were removed using size-exclusion chromatography with a S200 sephadex column (GE Healthcare, UK). To incorporate the FAM-dye strands, the purified origami from above (50 µL, 20 nM) was added to the FAM-strand (0.3 µL, 50 µM) and mixed at room temperature for 4 h.

Fibers Functionalized with DNA Origami: The assembled fiber (100 µL, 1 µM, 1 eq. of linker, 1× TAE, and 42 mM $MgCl_2$) was pelleted and washed 3× via centrifugation. The fiber (100 µL) was added to the purified DNA origami smiley (15 eq. of FAM-dye strand, 10 µL, 20 nM, TAE pH 8.3, and 14 mM $MgCl_2$) at room temperature and left to mix for 2 h prior to CLSM imaging. The non-complexed origami was removed by pelleting the fibers and washing once via centrifugation. For AFM analysis, the nanotube (100 µL, 1 µM, 1 eq. of linker, 1× TAE, and 28 mM $MgCl_2$) was pelleted and washed 3× via centrifugation. The DNA solution (100 µL) was added to the purified DNA origami smiley (10 µL, 20 nM, TAE pH 8.3, and 14 mM $MgCl_2$) at room temperature and left to mix for 1 h prior. The DNA solution (20 µL) was deposited on freshly cleaved mica, after 2 min additional assembly buffer (80 µL) was added. Images were collected using a Multimode 8 atomic force microscope (Bruker Santa Barbara, CA, USA) in fluid tapping mode using a MSNL cantilever E tip (Bruker Santa Barbara, CA, USA).

Fibers Functionalized with Hydrophobic DNA Nanoparticles: The cholesterol modified strands (3.4 µL, 100 µM, in water) and helper strands (0.2 µL, 50 µM, in water) (see Table S5, Supporting Information) were added to M13mp18 (40 µL, 100 nM) (New England Biolabs, UK), 10× TAE pH 8.3, 140 mM $MgCl_2$ (10 µL), and deionized water (46.4 µL). The nanoparticles were assembled by heating to 95 °C for 2 min, then cooled to 4 °C for 10 min. The nanoparticles (10, 5 and 1 µL, 40 nM, TAE pH 8.3, and 14 mM $MgCl_2$) were added to the assembled fiber (40 µL, 1 µM, containing 0.05 eq. of linker, 50 nM, TAE pH 8.3, and 42 mM $MgCl_2$) at room temperature and left to mix for 1 h prior to imaging.

Fibers Functionalized with Neutral and Cationic Vesicles: For neutral vesicles, DMPC lipid (36.9 mM, 271 µL in chloroform), cholesterol (100 mM, 50 µL in chloroform) and Cy5 PE lipid (1 mM, 2 µL, in chloroform) were mixed in a glass vial (20 mL). The organic solvent was removed under vacuum for 20 min using a rotary evaporator (Buchi, UK). The thin film was hydrated in phosphate buffered saline (PBS) (1×, 1 mL) by vortexing vigorously and sonicating for 1 min. Next, the solution was centrifuged for 10 min at 16 k r.p.m., and the supernatant was removed (800 µL) and replaced with fresh PBS (800 µL). The pellet was re-suspended by vortexing for 1 min, the process was repeated two more times to isolate GUVs. For 1000, 400, and 100 nm vesicles, the vesicles were extruded though a 1000, 400, or 100 nm filter using a syringe extruder kit (Avanti Polar Lipids, US). The liquid was passed through the filter 15 times. The vesicles were used within 2 weeks, stored at room temperature, and vortexed for 2 s before use. For cationic vesicles, the process above was followed, except POPC lipid (10 mM, 100 µL in chloroform), DOTAP (10 mM, 40 µL in chloroform), and Cy5 PE lipid (0.8 mM, 0.2 µL, in chloroform) were mixed in a glass vial (20 mL) instead. To generate fibers coated with vesicles, the extruded vesicles (2, 0.2, or 0.02 µL) were added to the assembled fiber (1 µM, 20 µL) at room temperature and left to mix for 1 h prior to imaging.

Fiber Adhesion under Flow: A microfluidic dish (1 mm wide, 8 chambers, Ibidi, DE) was carefully filled with water (10 µL) ensuring no air bubbles were generated, and a small droplet was left protruding from the *cis* and *trans* openings. 6-carboxyfluorescein (5 µM) was added to the water to aid visualization of the dish surface in a separate fluorescence channel. The assembled DNA fiber (20 µL, 10 µM in 1× TAE pH 8.3, 42 mM $MgCl_2$, and 20 mM $CaCl_2$) was added to the *cis* well followed by binding buffer (100 µL, 1× TAE pH 8.3, 42 mM $MgCl_2$, and 20 mM $CaCl_2$). Next, the plane of the dish was identified using the 6-carboxyfluorescein channel. To initiate fiber flow and adhesion, binding buffer (25 µL) was added to the *trans* well. A CLSM time series was performed to a region of interest, scanning every second.

E. coli Culture: Under sterile conditions, *E. coli* K12 EGFP bacteria were grown overnight in LB at 37 °C shaking at 300 r.p.m., supplemented with kanamycin (50 µg mL^{-1}). The culture was then diluted 1:100 and re-grown at 37 °C shaking at 300 r.p.m. for 3 h to reach exponential growth phase. Next, the culture was diluted 1:10, and IPTG (1.0 mM) was added to express GFP, and the culture incubated for a further 2 h shaking at 300 r.p.m. to reach an optical density (OD) of 1 at 600 nm. The cells (1 mL) were centrifuged for 1 min at 16k r.p.m., the supernatant removed, and re-suspended in PBS (1 mL) by vortexing for 30 s. The washing step was repeated twice, and the cells re-suspended in the stated buffer system for type I alignment, or PBS (1 mL) for type II alignment and used within 1 h.

Magnesium and Calcium Ion Fiber Alignment under Flow: The procedure for fiber adhesion described above was followed. After 5 min of fiber adhesion from the *cis* to the *trans* well, the liquid in the *trans* well was removed to stop the flow (≈100 µL). The excess fiber in the *cis* well was removed by washing the well with buffer (5 × 50 µL, 1× TAE pH 8.3, and 42 mM $MgCl_2$, and where stated supplemented with 20 mM $CaCl_2$), always ensuring liquid (≈25 µL) was left in the *cis* well to prevent air bubble formation. Binding buffer (1× TAE pH 8.3, 42 mM $MgCl_2$, and where stated supplemented with 20 mM $CaCl_2$) was added to the *cis* well (sum volume 100 µL), and then to the *trans* well (70 µL), the small volume imbalance generated a slow flow from the *cis* to *trans* well. *E. coli* (10 µL, OD of 1 at 600 nm, in either 1× TAE pH 8.3, 42 mM $MgCl_2$, or supplemented with 20 mM $CaCl_2$, or 0.3 M KCl, and 15 mM tris pH 8.0, where stated) was added to the *cis* well. A time series video was collected 1 min after the addition of the *E. coli* cells, or end point analysis after 20 min of flow. Particle tracking analysis was conducted

using Trackmate software to monitor the binding movement.[47] For the cell competition experiment under flow, the same protocol was followed, except *E. coli* cells (10 µL, OD 1 at 600 nm, in PBS) were mixed with heparinized human WB (0.2 µL) then loaded onto the flow chamber.

DOTAP Coated Fibers with E. coli Alignment: The vesicle-loaded fiber (10 µL, 1 µM, in 1× TAE pH 8.3, 42 mM $MgCl_2$ with 0.2 µL MUV or SUV, and 1 mM lipid in PBS) was added to PBS (10 µL) containing BSA (0.01 mg mL^{-1}). The solution (10 µL) was deposited on a glass petri fluordish (35 mm, Ibidi, DE) and left to settle for 5 min. *E. coli* (1 µL, OD 1 at 600 nm, in PBS) was added to the top of the droplet and carefully mixed, after 30 min the fiber was imaged. Particle tracking was conducted using Trackmate software.[47] To confirm viability, time series analysis was performed by scanning once every min for 30 min at 37 °C.

E. coli Extracellular Fiber Mesh: The assembled DNA fiber (20 µL, 10 µM, in 1× TAE pH 8.3, 42 mM $MgCl_2$, and 20 mM $CaCl_2$) was added to a fluorodish (35 mm, Ibidi, DE) and left to settle for 5 min. *E. coli* cells (0.2 µL, OD 1 at 600 nm, in PBS) were added to the top of the droplet. The images were collected after 10 min of incubation at room temperature.

E. coli Cell 1D Growth: The assembled DNA fiber (40 µL, 1 µM in 1× TAE pH 8.3, 42 mM $MgCl_2$, and 20 mM $CaCl_2$) was pipetted on to glass petri dish with lid (35 mm diameter, Ibidi, DE) and left to settle for 5 min. *E. coli* cells (0.6 µL, OD 1 at 600 nm, in PBS) were added to the top of the droplet and the dish incubated at 37 °C. Images were collected after 4 h by carefully transferring the dish on to the imaging platform.

Supporting Information

Supporting Information is available from the Wiley Online Library or from the author.

Acknowledgements

Prof. Stefan Howorka for kindly providing laboratory equipment and support. Prof. Mervyn Singer and Dr. Nishkantha Arulkumaran for providing healthy volunteer human blood. Experiments with human blood samples were approved by UCL research ethics committee (Reference: 11963/001); all experiments followed local procedures. The author was supported by the Rosetrees Trust (grant number M923).

Conflict of Interest

The author declares no conflict of interest.

Data Availability Statement

Data available on request from the authors & Data available in article supplementary material.

Keywords

condensation, DNA nanotechnology, fibers, macromolecular nanoarchitectonics, nanotubes

Received: January 10, 2021
Revised: March 12, 2021
Published online:

[1] N. C. Seeman, H. F. Sleiman, *Nat. Rev. Mater.* **2017**, *3*, 17068.
[2] P. W. K. Rothemund, *Nature* **2006**, *440*, 297.
[3] T. Gerling, K. F. Wagenbauer, A. M. Neuner, H. Dietz, *Science* **2015**, *347*, 1446.
[4] J. R. Burns, A. Seifert, N. Fertig, S. Howorka, *Nat. Nanotechnol.* **2016**, *11*, 152.
[5] S. M. Douglas, I. Bachelet, G. M. Church, *Science* **2012**, *335*, 831.
[6] a) Q. Jiang, S. Liu, J. Liu, Z. G. Wang, B. Ding, *Adv. Mater.* **2019**, *31*, 1804785; b) J. Chao, H. Liu, S. Su, L. Wang, W. Huang, C. Fan, *Small* **2014**, *10*, 4626.
[7] G. Yao, F. Zhang, F. Wang, T. Peng, H. Liu, E. Poppleton, P. Sulc, S. Jiang, L. Liu, C. Gong, X. Jing, X. Liu, L. Wang, Y. Liu, C. Fan, H. Yan, *Nat. Chem.* **2020**, *12*, 1067.
[8] K. F. Wagenbauer, C. Sigl, H. Dietz, *Nature* **2017**, *552*, 78.
[9] Z. Zhang, Y. Yang, F. Pincet, M. C. Llaguno, C. Lin, *Nat. Chem.* **2017**, *9*, 653.
[10] G. Tikhomirov, P. Petersen, L. Qian, *Nature* **2017**, *552*, 67.
[11] a) M. Komiyama, K. Yoshimoto, M. Sisido, K. Ariga, *Bull. Chem. Soc. Jpn.* **2017**, *90*, 967; b) K. Ariga, M. Nishikawa, T. Mori, J. Takeya, L. K. Shrestha, J. P. Hill, *Sci. Technol. Adv. Mater.* **2019**, *20*, 51.
[12] a) E. Akbari, M. Y. Mollica, C. R. Lucas, S. M. Bushman, R. A. Patton, M. Shahhosseini, J. W. Song, C. E. Castro, *Adv. Mater.* **2017**, *29*, 1703632; b) C. J. Kearney, C. R. Lucas, F. J. O'Brien, C. E. Castro, *Adv. Mater.* **2016**, *28*, 5509; c) Y. T. E. Chiu, H. Li, C. H. J. Choi, *Small* **2019**, *15*, 1805416.
[13] P. W. K. Rothemund, A. Ekani-Nkodo, N. Papadakis, A. Kumar, D. K. Fygenson, E. Winfree, *J. Am. Chem. Soc.* **2004**, *126*, 16344.
[14] a) D. Liu, S. H. Park, J. H. Reif, T. H. LaBean, *Proc. Natl. Acad. Sci. U. S. A.* **2004**, *101*, 5; b) D. Lubrich, J. Bath, A. J. Turberfield, *Nanotechnology* **2005**, *16*, 1574; c) P. O'Neill, P. W. K. Rothemund, A. Kumar, D. K. Fygenson, *Nano Lett.* **2006**, *6*, 1379; d) X. Liu, Y. Zhao, P. Liu, L. Wang, J. Lin, C. Fan, *Angew. Chem., Int. Ed.* **2019**, *58*, 8996; e) P. K. Lo, P. Karam, F. A. Aldaye, C. K. McLaughlin, G. D. Hamblin, G. Cosa, H. F. Sleiman, *Nat. Chem.* **2010**, *2*, 319; f) O. I. Wilner, R. Orbach, A. Henning, C. Teller, O. Yehezkeli, M. Mertig, D. Harries, I. Willner, *Nat. Commun.* **2011**, *2*, 540; g) A. M. Mohammed, R. Schulman, *Nano Lett.* **2013**, *13*, 4006; h) A. M. Maier, W. Bae, D. Schiffels, J. F. Emmerig, M. Schiff, T. Liedl, *ACS Nano* **2017**, *11*, 1301.
[15] H. Liu, Y. Chen, Y. He, A. E. Ribbe, C. Mao, *Angew. Chem., Int. Ed.* **2006**, *45*, 1942.
[16] P. Yin, R. F. Hariadi, S. Sahu, H. M. Choi, S. H. Park, T. H. Labean, J. H. Reif, *Science* **2008**, *321*, 824.
[17] K. M. Carneiro, N. Avakyan, H. F. Sleiman, *WIREs Nanomed. Nanobiotechnol.* **2013**, *5*, 266.
[18] D. Schiffels, T. Liedl, D. K. Fygenson, *ACS Nano* **2013**, *7*, 6700.
[19] R. Schreiber, N. Luong, Z. Fan, A. Kuzyk, P. C. Nickels, T. Zhang, D. M. Smith, B. Yurke, W. Kuang, A. O. Govorov, T. Liedl, *Nat. Commun.* **2013**, *4*, 2948.
[20] H. Bui, C. Onodera, C. Kidwell, Y. Tan, E. Graugnard, W. Kuang, J. Lee, W. B. Knowlton, B. Yurke, W. L. Hughes, *Nano Lett.* **2010**, *10*, 3367.
[21] R. Jungmann, M. S. Avendano, J. B. Woehrstein, M. Dai, W. M. Shih, P. Yin, *Nat. Methods* **2014**, *11*, 313.
[22] a) K. M. M. Carneiro, F. A. Aldaye, H. F. Sleiman, *J. Am. Chem. Soc.* **2010**, *132*, 679; b) N. Avakyan, A. A. Greschner, F. Aldaye, C. J. Serpell, V. Toader, A. Petitjean, H. F. Sleiman, *Nat. Chem.* **2016**, *8*, 368.
[23] a) I. Koltover, K. Wagner, C. R. Safinya, *Proc. Natl. Acad. Sci. U. S. A.* **2000**, *97*, 14046; b) V. A. Bloomfield, *Biopolymers* **1997**, *44*, 269.
[24] G. Pardatscher, D. Bracha, S. S. Daube, O. Vonshak, F. C. Simmel, R. H. Bar-Ziv, *Nat. Nanotechnol.* **2016**, *11*, 1076.
[25] J. R. Burns, K. Gopfrich, J. W. Wood, V. V. Thacker, E. Stulz, U. F. Keyser, S. Howorka, *Angew. Chem., Int. Ed.* **2013**, *52*, 12069.
[26] J. R. Burns, S. Howorka, *ACS Nano* **2018**, *12*, 3263.
[27] A. Ott, M. Magnasco, A. Simon, A. Libchaber, *Phys. Rev. E: Stat., Nonlinear, Soft Matter Phys.* **1993**, *48*, R1642.
[28] T. Nguyen, A. Brewer, E. Stulz, *Angew. Chem., Int. Ed.* **2009**, *48*, 1974.

[29] A. Ekani-Nkodo, A. Kumar, D. K. Fygenson, *Phys. Rev. Lett.* **2004**, *93*, 268301.
[30] S. Marton, F. Cleto, M. A. Krieger, J. Cardoso, *PLoS One* **2016**, *11*, e0153637.
[31] I. Willner, B. Shlyahovsky, M. Zayats, B. Willner, *Chem. Soc. Rev.* **2008**, *37*, 1153.
[32] M. M. Ali, F. Li, Z. Zhang, K. Zhang, D. K. Kang, J. A. Ankrum, X. C. Le, W. Zhao, *Chem. Soc. Rev.* **2014**, *43*, 3324.
[33] A. Akbarzadeh, R. Rezaei-Sadabady, S. Davaran, S. W. Joo, N. Zarghami, Y. Hanifehpour, M. Samiei, M. Kouhi, K. Nejati-Koshki, *Nanoscale Res. Lett.* **2013**, *8*, 102.
[34] a) H. Mulcahy, L. Charron-Mazenod, S. Lewenza, *PLoS Pathog.* **2008**, *4*, e1000213; b) T. W. Halverson, M. Wilton, K. K. Poon, B. Petri, S. Lewenza, *PLoS Pathog.* **2015**, *11*, e1004593.
[35] R. F. Epand, P. B. Savage, R. M. Epand, *Biochim. Biophys. Acta* **2007**, *1768*, 2500.
[36] Z. Wang, Y. Ma, H. Khalil, R. Wang, T. Lu, W. Zhao, Y. Zhang, J. Chen, T. Chen, *Int. J. Nanomed.* **2016**, *11*, 4025.
[37] O. Birkholz, J. R. Burns, C. P. Richter, O. E. Psathaki, S. Howorka, J. Piehler, *Nat. Commun.* **2018**, *9*, 1521.
[38] J. Xie, M. Bao, S. M. C. Bruekers, W. T. S. Huck, *ACS Appl. Mater. Interfaces* **2017**, *9*, 19630.
[39] a) A. Devaraj, J. R. Buzzo, L. Mashburn-Warren, E. S. Gloag, L. A. Novotny, P. Stoodley, L. O. Bakaletz, S. D. Goodman, *Proc. Natl. Acad. Sci. U. S. A.* **2019**, *116*, 25068; b) R. Pakkulnan, C. Anutrakunchai, S. Kanthawong, S. Taweechaisupapong, P. Chareonsudjai, S. Chareonsudjai, *PLoS One* **2019**, *14*, e0213288.
[40] V. P. Ma, K. Salaita, *Small* **2019**, *15*, 1900961.
[41] L. Liu, S. Chen, Z. Xue, Z. Zhang, X. Qiao, Z. Nie, D. Han, J. Wang, T. Wang, *Nat. Commun.* **2018**, *9*, 444.
[42] M. Okshevsky, R. L. Meyer, *Crit. Rev. Microbiol.* **2015**, *41*, 341.
[43] M. Trokter, C. Felisberto-Rodrigues, P. J. Christie, G. Waksman, *Curr. Opin. Struct. Biol.* **2014**, *27*, 16.
[44] a) S. R. Caliari, J. A. Burdick, *Nat. Methods* **2016**, *13*, 405; b) R. Freeman, M. Han, Z. Álvarez, J. A. Lewis, J. R. Wester, N. Stephanopoulos, M. T. McClendon, C. Lynsky, J. M. Godbe, H. Sangji, E. Luijten, S. I. Stupp, *Science* **2018**, *362*, 808.
[45] a) J. Gačanin, C. V. Synatschke, T. Weil, *Adv. Funct. Mater.* **2019**, *30*, 1906253; b) E. Lattuada, M. Leo, D. Caprara, L. Salvatori, A. Stoppacciaro, F. Sciortino, P. Filetici, *Front. Pharmacol.* **2020**, *11*, 01345.
[46] J. S. Graham, B. R. McCullough, H. Kang, W. A. Elam, W. Cao, E. M. De La Cruz, *PLoS One* **2014**, *9*, e94766.
[47] J. Y. Tinevez, N. Perry, J. Schindelin, G. M. Hoopes, G. D. Reynolds, E. Laplantine, S. Y. Bednarek, S. L. Shorte, K. W. Eliceiri, *Methods* **2017**, *115*, 80.